

# Porous cholesteric liquid crystal film-integrated optical fiber sensor for real-time detection of high-concentration volatile organic compounds



Soyeon Ahn <sup>a,1</sup>, Nahyeon Hwang <sup>a</sup>, Min Su Kim <sup>a</sup>, Ji Su Kim <sup>a,2</sup>, Byeong Kwon Choi <sup>a,1</sup>, Sung Yoon Cho <sup>a</sup>, Jaehyun Yoo <sup>a</sup>, Na-Hyun Bak <sup>a</sup>, Minjun Kim <sup>b</sup>, Jong-Hyun Kim <sup>a,b</sup>, Moon-Deock Kim <sup>a,b</sup>, Min Yong Jeon <sup>a,b,\*</sup>

<sup>a</sup> Department of Physics, Chungnam National University, 99 Daehak-ro, Yuseong-gu, Daejeon 34134, Republic of Korea

<sup>b</sup> Institute of Quantum Systems (IQS), Chungnam National University, 99 Daehak-ro, Yuseong-gu, Daejeon 34134, Republic of Korea

## ARTICLE INFO

### Keywords:

Cholesteric liquid crystal film (CLCF)  
Volatile organic compounds sensor  
Wavelength-swept laser  
Gas sensor  
Fiber-optic sensor

## ABSTRACT

Real-time detection of flammable volatile organic compounds (VOCs) vapors is essential for ensuring safety in various industrial environments. This paper presents a compact, all-fiber sensor designed for real-time monitoring of high concentration of flammable VOC vapors. The sensor is fabricated by coating a porous cholesteric liquid crystal film (CLCF) onto the cross-section of an optical fiber ferrule. An ultra-wideband, high-speed wavelength-swept laser (WSL) is employed to monitor shifts in the reflection band of the CLCF in response to varying concentrations of benzene, toluene, and acetone vapors. Sensitivities of 6.11 pm/ppm, 4.48 pm/ppm, and 3.19 pm/ppm were achieved for benzene, toluene, and acetone vapors, respectively, with the highest sensitivity observed for benzene. By leveraging the one-to-one correspondence between spectral and temporal domains, the sensor enables real-time vapor concentration measurements. The device demonstrated excellent repeatability, with a standard deviation of 0.228 nm in the reflection band center wavelength after five exposures to 25 % of the lower explosive limit of benzene vapor. Additionally, the porous CLCF exhibited approximately six times greater sensitivity than its nonporous counterpart. The sensor also features low dependence on temperature and humidity, operates without a battery, and is immune to electromagnetic interference. These results underscore the potential of the proposed sensor as a reliable and practical solution for flammable VOC vapor detection. Furthermore, an analysis of the porous CLCF's vapor sensing mechanism reveals that the high sensitivity to benzene is attributed to its porous structure and benzene's high refractive index.

## 1. Introduction

Flammable liquids, particularly volatile organic compounds (VOCs), are widely used in various industrial applications. The evaporation of VOCs can lead to flammable vapor concentrations in air, where even a small ignition source may result in combustion or explosion. Therefore, accurate real-time monitoring of vapor concentrations is crucial for ensuring safety. A wide range of flammable VOC sensors has been developed [1–6]. Among them, catalytic combustion sensors and semiconductor gas sensors are commonly used due to their high sensitivity, linear response to gas concentration, ease of operation, and low cost. However, these sensors are vulnerable to environmental interferences such as humidity, temperature fluctuations, and electromagnetic fields.

Moreover, they typically require high operating temperatures ( $> 100^{\circ}\text{C}$ ) and external power sources, as optimal gas detection is achieved only under specific thermal conditions [5,6].

Cholesteric liquid crystals (CLCs) are characterized by a periodic structure with a helical twist structure and have unique optical properties of selective reflection that reflect incident wavelengths, and the pitch corresponding to one period is very sensitive to external stimuli, making them useful in various sensing devices [7–12]. However, CLCs require a supporting substrate due to their fluid properties and are mechanically unstable, so CLC films (CLCFs) that form polymer networks by incorporating reactive mesogens (RMs) into CLCs have been extensively studied [13–16]. These CLCFs offer excellent mechanical and thermal stability, and have a larger surface area than conventional

\* Corresponding author at: Department of Physics, Chungnam National University, 99 Daehak-ro, Yuseong-gu, Daejeon 34134, Republic of Korea.

E-mail address: [myjeon@cnu.ac.kr](mailto:myjeon@cnu.ac.kr) (M.Y. Jeon).

<sup>1</sup> Siemens Electronic Design Automation, 192-gil 12, Pangyoek-ro, Bundang-gu, Seongnam-si, Gyeonggi-do 13524, Republic of Korea.

CLCs, which improves their interaction with the external environment, making them suitable for gas sensing applications. Unlike gas sensors based on catalytic combustion or semiconductor mechanisms, which require high operating temperatures and external power, CLCF-based optical sensors operate at room temperature without the need for external power or heating and exhibit excellent resistance to environmental variations such as humidity and thermal fluctuations [5,6]. Moreover, optical fiber sensors are inherently immune to electromagnetic interference and operate without the need for external power sources, making them well-suited for a wide range of sensing applications, including temperature, humidity, pressure, and gas detection [17–32]. In particular, gas sensors have been developed through various approaches, such as combining them with carbon nanotubes or graphene [23,24], utilizing optical fiber structures such as fiber Bragg gratings or hollow-core fibers [25,26], long-period fiber Bragg gratings [27], applying interferometric techniques [29,30], and integrating them with liquid crystals (LCs) [13,31,32]. Among these, the porous CLCF-coated sensor exhibits intrinsic environmental robustness and ease of fabrication, setting it apart from conventional fiber-optic gas sensors that often require complex structural designs to ensure stable performance. Table 1 presents a comparison between conventional fiber-optic gas sensors and the porous CLCF-based fiber-optic gas sensor.

Several recent studies have demonstrated the effectiveness of CLCF-coated optical fibers in VOC sensing. In 2018, Tang et al., reported a VOC gas sensor combining side-polished optical fiber with a CLCF, achieving sensitivities of approximately 7.08 nm•L/mmol for tetrahydrofuran, 3.46 nm•L/mmol for acetone, and 0.52 nm•L/mmol for methanol [33]. In 2021, Hu et al., demonstrated an acetone gas sensor with a CLCF-coated optical fiber tip, showing a sensitivity of about 48.46 nm•L/mmol [31]. In 2022, Li et al., introduced an acetone vapor sensor using pre-compressed CLCF on an optical fiber tip, with a sensitivity of approximately 0.23 pm/ppm [32]. These studies have demonstrated that the sensor response to gas or vapor is highly linear. However, since the lower explosive limits (LELs) of many flammable VOC vapors occur at relatively high concentrations — typically ranging from 100 ppm to over 10,000 ppm — further investigation is required to evaluate sensor performance under these conditions. Although numerous studies have reported promising results for the detection of flammable VOC vapors, discussions regarding their practical applicability and potential advantages remain limited. Therefore, in-depth exploration on the applicability of these sensors in various industries, including chemical, petroleum, and pharmaceutical industries, are needed. In the petroleum industry, these sensors can monitor the accumulation of flammable vapors in fuel storage or during transportation to prevent hazardous ignition events, and in the chemical industry, they can act as early warning systems for leaks that may not be detected until the concentration of hazardous gases exceeds thresholds. A deeper analysis of such sector-specific scenarios would help

underscore the versatility and necessity of these sensors. The possibility of linking fiber-based sensors to automated safety mechanisms—such as fire suppression systems or ventilation controls—could further enhance real-time response to hazardous conditions.

In this paper, we propose, for the first time to our knowledge, a compact all-fiber flammable VOC gas sensor by coating the cross-section of an optical fiber ferrule with porous CLCF. The sensor is designed for real-time detection of high-concentration flammable vapors and employs an ultra-wideband, high-speed wavelength-swept laser (WSL) with a spectral bandwidth exceeding 440 nm. Reflection band shifts of the CLCF are monitored in response to varying concentrations of acetone, toluene, and benzene vapors, confirming the device's potential for vapor sensing. The sensor achieves sensitivities of 6.11 pm/ppm, 4.48 pm/ppm, and 3.19 pm/ppm for benzene, toluene, and acetone, respectively, with the highest sensitivity observed for benzene. By leveraging the one-to-one correspondence between spectral and temporal domains, the sensor enables real-time vapor concentration monitoring. The device exhibits excellent repeatability, with a standard deviation of 0.228 nm in the reflection band center wavelength after five exposures to 25 % of the lower explosive limit (LEL) of benzene vapor. A comparison between porous and nonporous CLCF shows that the porous structure offers approximately six times higher sensitivity to benzene vapor. Furthermore, unlike catalytic combustion or semiconductor-based gas sensors, this sensor exhibits low dependency on temperature and humidity, operates without the need for external power, and is immune to electromagnetic interference, demonstrating high practicality and reliability for VOC gas detection. The enhanced sensitivity to benzene is attributed to the increased surface area of the porous CLCF and the high refractive index of benzene, as revealed by analysis of the sensing mechanism.

## 2. Experiments

### 2.1. Materials

The nematic liquid crystal mixture E7 (a mixture of 5CB, 7CB, 9OCB, and 5CT), the RM 2-Methyl-1,4-phenylene bis(4-(3-(acryloyloxy)propoxy)benzoate (RM257), and the chiral dopant S-(+)-2-Octyl 4-(4-hexyloxybenzoyloxy)benzoate (S811) were purchased from QY Liquid Crystal Corp. The photo-initiator 1,2-Diphenyl-2,2-dimethoxyethanone (IRG651) and the cross-linker Trimethylolpropane triacrylate (TMPTA) were obtained from commercial suppliers and used as received. The polyamide solution was obtained from JNC Corp. Acetone, toluene, and benzene were purchased from Daejung Chemicals & Metals Co., Ltd. Nitrogen gas ( $N_2$ ) was purchased from World Enersys. The optical fibers (SMF-28, FC/UPC type) were purchased from East Photonics, Inc. The refractive indices of the core and cladding of SMF-28 are 1.45213 and 1.44692, respectively [34]. The mating sleeve was purchased from Thorlabs, Inc. All materials were used without further

**Table 1**  
Comparison of gas sensors combined with optical fibers.

Sensor type	Operating conditions	Environmental robustness	Sensitivity	Fabrication complexity
Carbon nanotubes [23]	Ambient pressure	Not reported	12 AU/ppm NH <sub>3</sub>	Low (Dropcast and dry method)
Graphene [24]	Ambient pressure	Thermally stable	4 pm/ppm NH <sub>3</sub> (< 100 ppm)	Moderate (CVD graphene + fiber micro-etch)
Fiber Bragg gratings [25]	Often needs thermal control; ambient pressure	Active temperature modulation required	$2.2 \times 10^{-6}$ dB/ppm C <sub>2</sub> H <sub>2</sub>	High (Stack and draw method)
Hollow-core fibers [26]	$\Delta P \sim 0.8$ bar for fast gas filling	Not reported	LoD = 0.4 ppm CO	High (HC-NCF fabrication & free-space coupling)
Long-period fiber Bragg grating [27]	Optical RH 57–75 %; ambient pressure	Humidity-dependent (optimum band)	98.32 pm/ppm (0–8 ppm) NH <sub>3</sub>	Low (Dip-coating method)
Photothermal SMF-FPI [29]	Ambient pressure	Excellent resistance to humidity and temperature variations	LoD = 45 ppb C <sub>2</sub> H <sub>2</sub>	Low (cleave two SMFs + insert sleeve)
Chitosan/PDMS interferometer [30]	Ambient pressure	Sensitive to humidity and temperature	7.6 pm/ppm formic acid	Moderate (dip coating + PDMS overlayer)
Porous-CLCF [This work]	Ambient pressure	Excellent resistance to humidity and temperature variations	6.11 pm/ppm benzene	Low (Simple tip coating; no microfabrication)

purification or processing, except for the mating sleeve, which was modified by drilling a central hole using a coring drill bit to enable capillary-driven infiltration of the CLCF precursor.

## 2.2. Fabrication of a porous CLCF coated optical fiber device

**Fig. 1** depicts the fabrication process of the sensor device. The cross-sections of two optical fiber ferrules were first coated with a thin layer of polyamide solution and cured in an oven at 60 °C for approximately 1.5 h, forming a polyimide coating. The surfaces were then treated by rubbing them in a specific direction with a velvet cloth to ensure horizontal alignment of the LCs. The two ferrules were aligned using a mating sleeve, leaving a gap of about 100 μm between them. The CLCF precursor was injected into this gap and exposed to UV light (@325 nm) at an intensity of about 30 mW/cm<sup>2</sup> for 10 min to coat the ferrule cross-sections with CLCF. Following this, the CLCF-coated ferrules were immersed in acetone for 30 min to remove non-reactive materials. In this study, both porous and nonporous CLCF devices were fabricated, and their properties were compared.

The pitch of the porous CLCF decreases with the ratio of non-reactive material, and the initial pitch is described by the equation:

$$P_{init} = \frac{1}{HTP \times C_{CD}} \quad (1)$$

$$\lambda_{c,porous} \cong \lambda_{c,init} \cdot \left(1 - \frac{C_{NRM}}{100}\right) \quad (2)$$

where  $P_{init}$  [7] represents the initial porous CLCF pitch,  $\lambda_{c,init}$  and  $\lambda_{c,porous}$  [Supplementary material S1] are the wavelength of the initial and porous CLCF,  $HTP$  is the helical twisting power of the chiral dopant, and  $C_{CD}$  and  $C_{NRM}$  are the concentrations of the chiral dopant and non-reactive material, respectively. To fabricate porous and nonporous CLCFs with reflection centered in the 1300 nm band, two types of precursor mixtures, designated as precursor A and precursor B, were prepared with specific compositions. Precursor A consisted of E7 (62.6 wt %), RM257 (24.6 wt%), S811 (3.5 wt%), TMPTA (5.3 wt%), and IRG651 (1.0 wt%). Precursor B comprised E7 (57.6 wt%), RM257 (24.7 wt%), S811 (11.8 wt%), TMPTA (4.9 wt%), and IRG651 (1.0 wt %). The initial cholesteric pitch values calculated for precursors A and B were 2.6 μm and 0.77 μm, respectively. After the formation of porosity, the cholesteric pitch of porous CLCF A was reduced to approximately

0.80 μm. When the concentration of RM257 is reduced to approximately 15 wt%, phase separation occurs during UV curing. Conversely, when the concentration exceeds 45 wt%, the mixture retains a crystalline phase at room temperature, which hinders the UV curing process. The lower concentration of RM257 leads to the higher pore density, which is anticipated to enhance the effective surface area available for interactions with the external environment [as illustrated in **Fig. S2** in Supplementary material S2]. Considering these factors, an RM257 concentration of 24.7 wt% was selected for the experimental studies conducted in this work.

**Fig. 2(a)** shows the FTIR spectra of the nonporous and porous CLCF samples measured by a vacuum infrared spectrometer (VERTEX 80v). Dips for nonporous CLCF were observed at 2927, 2225, 1726, and 1604 cm<sup>-1</sup>, and these dips represent the molecular bonds of C–H, C–N, C–O, and C–C, respectively. In contrast, for the porous CLCF, dips were observed at 2960, 1724, and 1604 cm<sup>-1</sup>, and it can be confirmed that only the dip for the C–N bond has disappeared. **Fig. 2(b)** shows a cross-sectional SEM image of the porous CLCF, clearly confirming the formation of pores. As shown in **Fig. 2(c)**, since E7 is the only material among those used in this study that has a C–N bond, it was confirmed that the porous CLCF was well formed.

## 2.3. Experimental setup

**Fig. 3** presents a schematic of the experimental setup used to measure the response of the CLCF device to analyte vapors. A wideband WSL with a broad scanning range of approximately 443 nm (1131–1574 nm) and a 10 dB bandwidth was employed as the light source. This realized a wideband WSL light source by sharing one wavelength scanning filter with two resonators (center wavelengths of 1.25 μm and 1.45 μm). The operating principles and generation of light sources are well described in the Refs. [9,35]. The WSL is well-suited for real-time dynamic sensors due to its wide wavelength range, stable spectrum, and one-to-one correspondence between the spectral and temporal domains.

Since the device only reflects circularly polarized light, two polarization controllers were used to adjust the polarization state of the incident beam, optimizing the reflectivity within the reflection band. An optical circulator directed the output from the WSL to the sensing device inside the gas chamber and measured the beam reflected from the device. A 90:10 fiber coupler split the reflected signal, with 10 % of the beam monitored by an oscilloscope and the remaining 90 % analyzed by

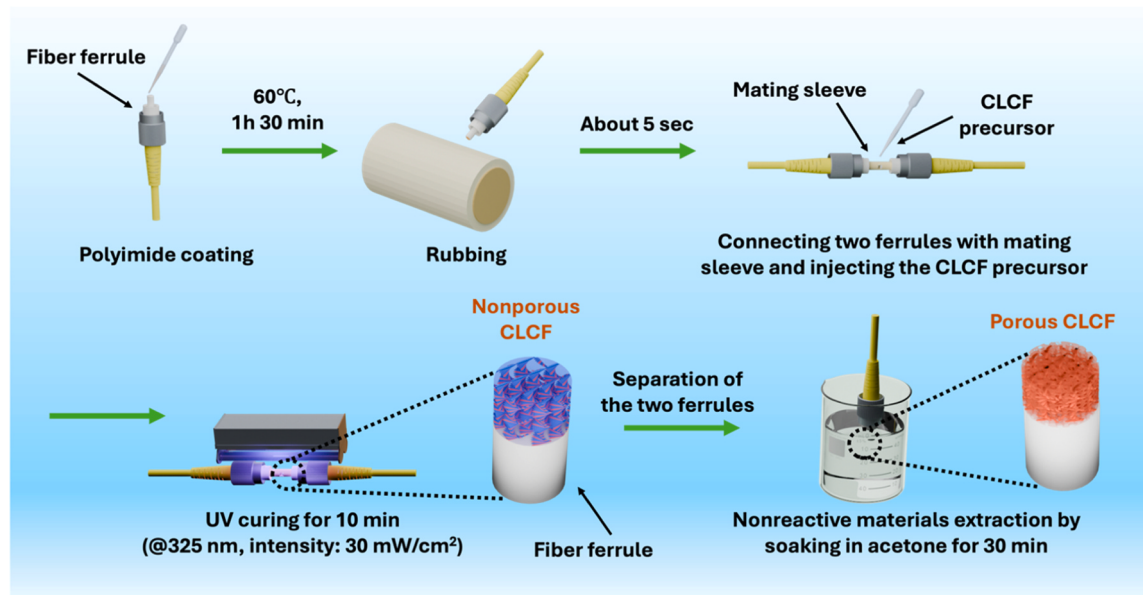


**Fig. 1.** Schematic illustration of the fabrication process of the porous CLCF device.

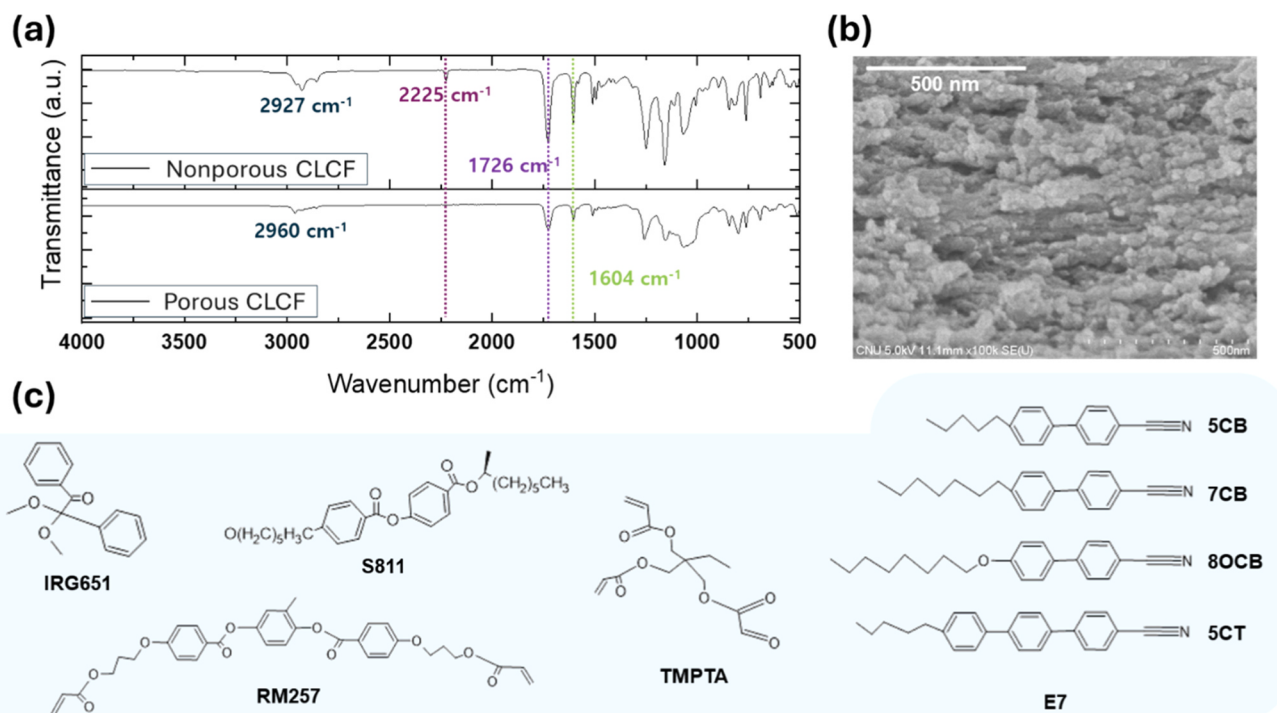


Fig. 2. (a) FTIR of nonporous and porous CLCFs, (b) SEM image of the porous CLCF and (c) molecular structures of IRG651, S811, RM257, TMPTA and E7.

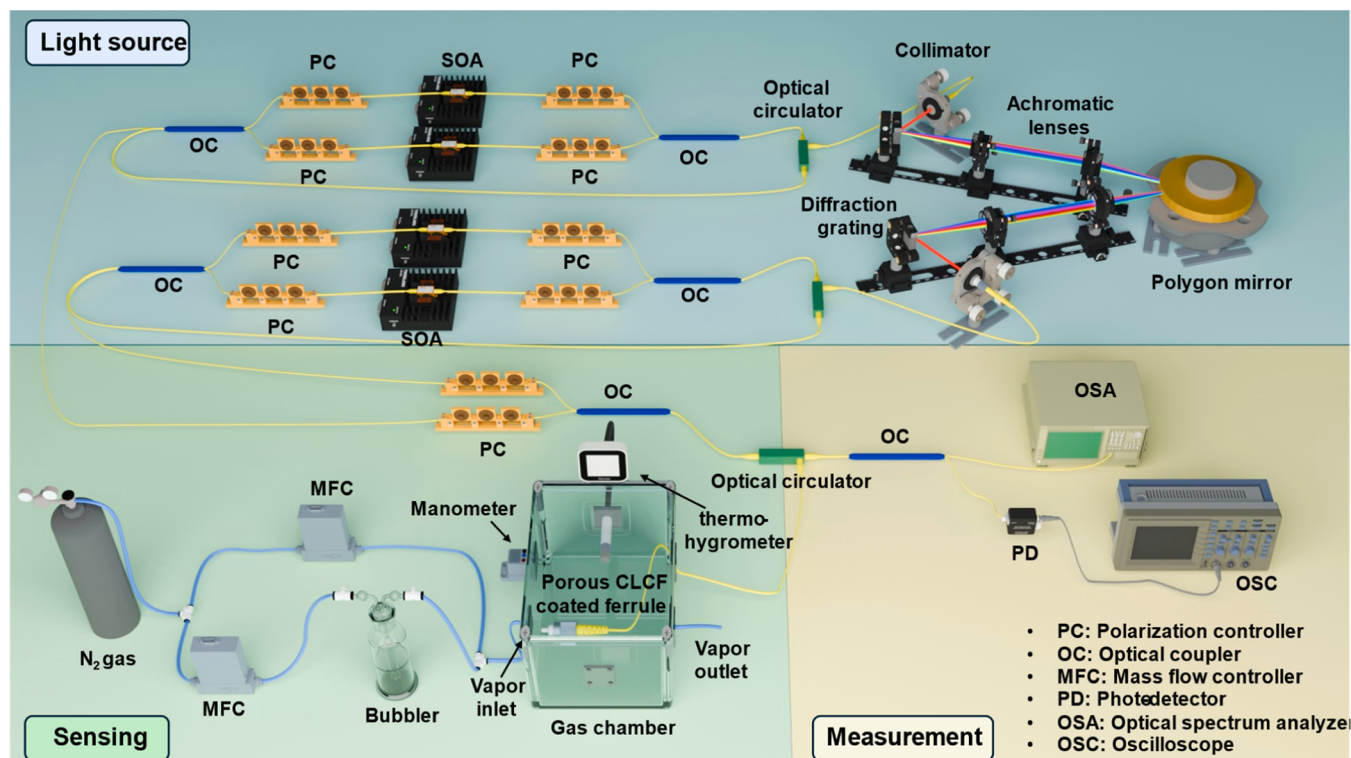


Fig. 3. Schematic of the experimental setup for measuring the response of CLCF devices to analyte vapors. OC: optical coupler; PC: polarization controller; SOA: semiconductor optical amplifier; OSA: optical spectrum analyzer; MFC: mass flow controller; OSC: oscilloscope.

an optical spectrum analyzer (OSA). The sensing device was housed within a gas chamber (24°C, 30 %R.H., @ 1 atm), and vapor concentrations were controlled by adjusting the volume ratio of N<sub>2</sub> gas to the analyte vapor using mass flow controllers (MFCs). This setup allowed for the injection of various vapor concentrations to monitor the sensor's

response. After each test, pure N<sub>2</sub> gas was injected into the chamber to confirm the recovery of the device.

## 2.4. Vapor generation

The vapors used in the experiment — benzene, toluene, and acetone — are all liquids at room temperature. To generate high concentrations of vapor, a bubbler was employed. The vapor concentration was first estimated under the assumption that the air pressure in the chamber remained at 1 atm. A thermo-hygrometer and a manometer were used to measure the temperature and pressure, respectively. Since the vapor pressure existing the bubbler varies with temperature and pressure, the vapor concentration was measured as a function of flow rate using a commercial gas sensor (MP400P), capable of measuring concentrations up to 10,000 ppm. The vapor pressure of each substance was then calculated. The volume ratio of vapor produced by the bubbler is given by the equation:

$$y_i = \frac{P_v}{P_T} \quad (3)$$

where  $y_i$  is the volume ratio of vapor produced,  $P_v$  is the vapor pressure and  $P_T$  is the total pressure. The concentration of vapor as a function of flow rate was calculated using the following equation:

$$C \text{ (ppm)} = \frac{\nu_1 \times y_i}{\nu_1 + \nu_2} \times 10^6 \quad (4)$$

where  $\nu_1$  is the flow rate of pure N<sub>2</sub> gas, and  $\nu_2$  is the flow rate of N<sub>2</sub> gas passing through the bubbler [36]. To obtain the gas concentration,  $\nu_1$  and  $\nu_2$  represent the flow rates adjusted using the MFC,  $P_T$  is set at 101.3 kPa (1.0 atm), and the vapor pressures  $P_v$  of acetone, toluene, and benzene are 13.9 kPa, 3.4 kPa, and 6.5 kPa, respectively. Owing to the practical flow rate limitation of the MFC ( $\geq 25$  sccm), the lowest achievable vapor concentrations were approximately 5500 ppm for acetone and around 3000 ppm for benzene and toluene.

## 2.5. Characteristics of WSL

Fig. 4(a) and (b) show the output of the WSL in the spectral and temporal domains, respectively. The 10-dB scanning bandwidth of the WSL is approximately 443 nm in the spectral domain and 328  $\mu$ s in the temporal domain. The shapes are similar with each other. The WSL provides a one-to-one correspondence between the spectral and temporal domains, where 1  $\mu$ s in the temporal domain corresponds to approximately 1.35 nm in the spectral domain [35]. Here, the wideband WSL combines two wavelength bands, 1.25  $\mu$ m and 1.45  $\mu$ m, using a single polygon scanner-based wavelength filter.

## 3. Results and discussion

### 3.1. Real-time response to the benzene, toluene, and acetone vapors

Fig. 5(a) and (b) display the reflection spectra of the sensor in response to varying concentrations of benzene, toluene, and acetone vapors in spectral domain and temporal domains, respectively. As shown in Fig. 5(a), as the vapor concentration increased, the center wavelength of the reflection spectra shifted toward longer wavelengths. Specifically, for benzene vapor, the wavelength shifted from 1323.4 nm to 1386.0 nm (a shift of 62.6 nm) as the concentration increased from 0 to 10.3k ppm. For toluene vapor, the shift was from 1330.0 nm to 1378.2 nm (48.2 nm) over the range of 0–10.4k ppm. In the case of acetone vapor, the wavelength shifted from 1313.2 nm to 1381.0 nm (67.8 nm) as the concentration increased from 0 to 20.6k ppm. As shown in Fig. 5(b), the spectra measured in the temporal domain shift toward the right with increasing vapor concentration, consistent with the trends observed in the spectral domain. Fig. 5(c)–(e) illustrate the relationship between vapor concentration and the center wavelength for benzene, toluene, and acetone vapors in both the spectral and temporal domains.

The central peak shifts in the temporal domain were precisely converted to wavelength shifts based on the established correlation between the temporal and spectral domains of the WSL output, as shown in Fig. 4. The center wavelength was defined as the midpoint of the 6-dB bandwidth of the reflection band. Linear fitting analysis in the spectral domain yielded sensitivities of 6.11 pm/ppm, 4.48 pm/ppm, and 3.19 pm/ppm for benzene, toluene, and acetone vapors, respectively. Based on their respective LELs of 12,000 ppm, 11,000 ppm, and 22,000 ppm, the sensitivities correspond to 0.733, 0.493, and 0.702 nm/%LEL for benzene, toluene, and acetone, respectively [37–39]. This conversion facilitates the evaluation of sensor performance in terms of %LEL, thereby providing a more practical metric for assessing the sensor's applicability to safety-critical vapor concentrations. Sensitivity is defined as the rate of change in the reflection peak wavelength with respect to vapor concentration, expressed as  $S = \frac{d\lambda}{dC}$  [40]. In the temporal domain, the corresponding sensitivities obtained from linear fitting were 5.97 pm/ppm, 4.25 pm/ppm, and 3.05 pm/ppm. The coefficients of determination ( $R^2$ ) were 0.986, 0.960, and 0.998 for benzene, toluene, and acetone in the spectral domain, and 0.981, 0.965, and 0.998 in the temporal domain, respectively. These high  $R^2$  values confirm strong linear correlations between vapor concentration and wavelength shift. Error bars were included to reflect measurement uncertainties, accounting for minor instrumentation error from the broadband WSL, as well as variations in measurement resolution and intensity.

The results presented in this study are based on a device with a thickness of 100  $\mu$ m. To examine the effect of reduced thickness, an additional device with a thickness of 31  $\mu$ m was fabricated, and its

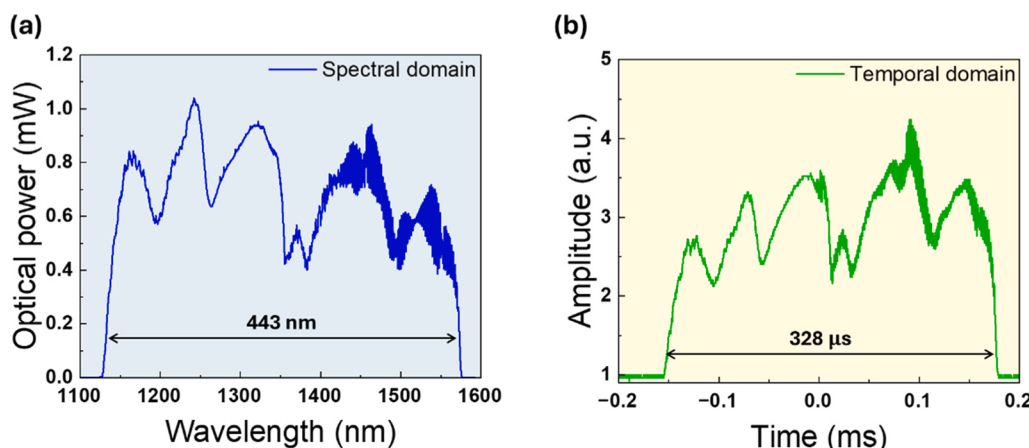
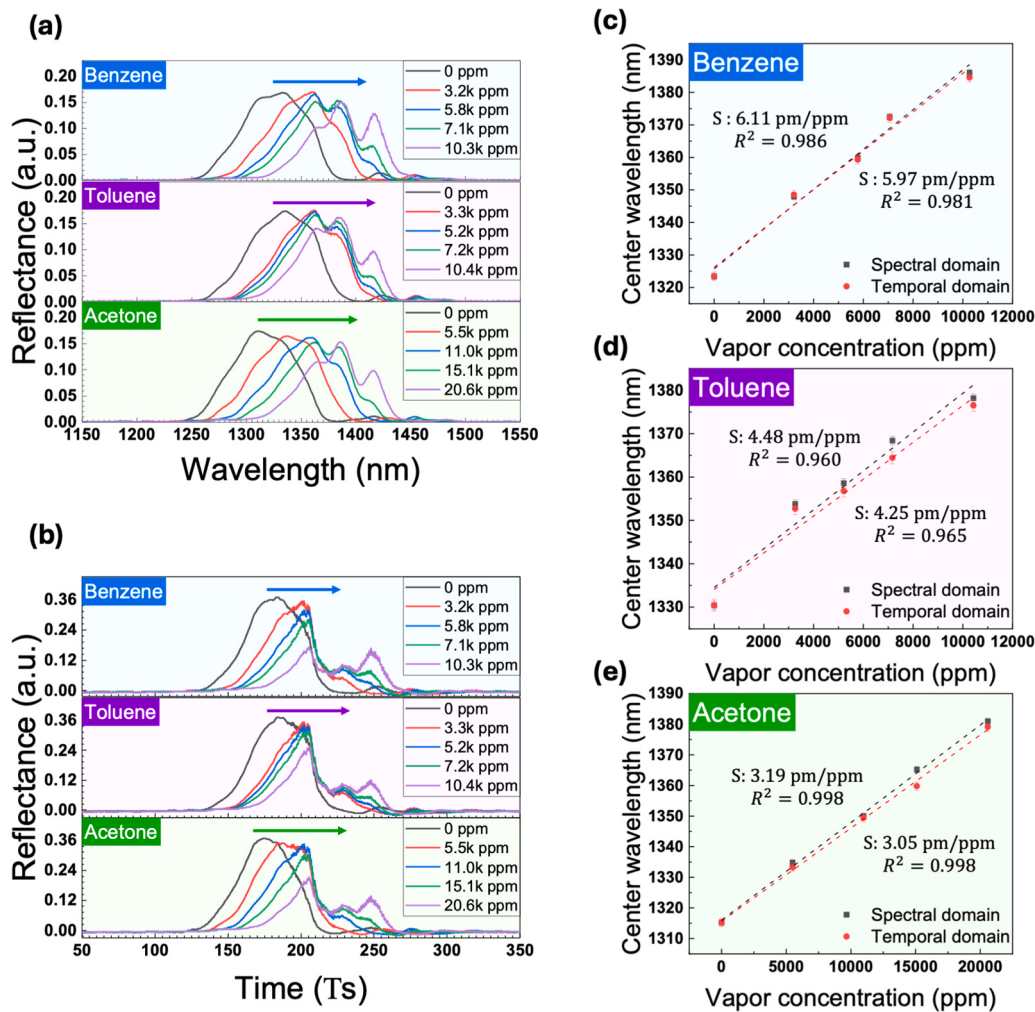


Fig. 4. WSL outputs in the (a) spectral and (b) temporal domain.



**Fig. 5.** (a) Spectral and (b) temporal variations in the reflectance spectra in response to different vapor concentrations of benzene, toluene, and acetone vapors. (c–e) Linearity comparison of center peak shifts in the reflection bands between spectral and temporal domains for (c) benzene, (d) toluene, and (e) acetone.

sensitivity to benzene vapor was evaluated. As detailed in [Supplementary material S3](#), the thinner device exhibited a sensitivity of approximately 1.81 pm/ppm, which is about 3.3 times lower than that of the 100  $\mu\text{m}$ -thick device. Nevertheless, it still demonstrated a clear and linear response.

Considering the LEL of each vapor, the calculated limits of detection ( $LoD$ ) in the spectral domain were 12 % LEL, 22.3 % LEL, and 4.7 % LEL for benzene, toluene, and acetone, respectively. In the temporal domain, the corresponding  $LoD$  values were 14.1 % LEL, 20.6 % LEL, and 5.0 % LEL. The  $LoD$  was calculated using the equation  $LoD = \frac{3.3\sigma}{S}$ , where  $\sigma$  is the standard deviation of the baseline signal and  $S$  is the sensitivity. These results indicate that the sensor exhibits sufficient sensitivity to detect flammable VOC gas vapors. Moreover, the close agreement between the spectral and temporal domain measurements validates the feasibility of real-time and accurate vapor concentration detection using temporal domain signals.

[Fig. 6\(a\)](#) presents a comparison of the changes in the central peak of the reflection band with respect to acetone vapor concentration, as measured by both the commercial gas sensor and the fabricated sensor. The temporal variation in vapor concentration over a 10-min exposure, measured by the commercial gas sensor (MP400P, blue dotted line), shows a strong similarity to the shift in the central peak of the reflection band measured by the proposed device (black solid line) under the same conditions. Building on this similarity, [Fig. 6\(b\)](#) shows the time-domain response of the fabricated device, illustrating changes in the central peak

of the reflection band with respect to the vapor concentrations of benzene, toluene, and acetone. The response and recovery cycles were repeated at 10-min intervals for each vapor concentration. After the vapor was replaced with  $\text{N}_2$  gas, the central peak returned to nearly the same position as before the response, indicating recovery. The 90 % response and 10 % recovery times for all vapor concentrations ranged from 1 to 6 min, which are relatively long, and no distinct trends were observed with respect to vapor type or concentration. This may be attributed to the fact that the vapor concentration generated by the bubbler does not instantaneously reach the target level, as illustrated in [Fig. 6\(a\)](#). Although the response and recovery times could not be quantitatively extracted from the experimental data alone, the system behavior was effectively described using a first order plus dead time (FOPDT) model, which characterizes systems with a delayed response following an input change [41,42]. It is important to note that the reference sensor (MP400P) has its own intrinsic dynamic characteristics, making it difficult to treat the measured concentration as an ideal input. Nevertheless, the FOPDT model fitting showed good agreement with the actual sensor response, as demonstrated in [Fig. S4](#) [[Supplementary material S4](#)]. The parameters estimated from the model were a response time constant ( $\tau_{res}$ ) of 23.47 s and a recovery time constant ( $\tau_{rec}$ ) of 60.62 s. The shorter  $\tau_{res}$  compared to  $\tau_{rec}$  indicates that analyte molecules diffuse into and adsorb onto the porous structure more rapidly during the response phase than they desorb during the recovery phase, even under continuous  $\text{N}_2$  purging. This asymmetry suggests that some vapor molecules remain adsorbed on the surface or within the pores of

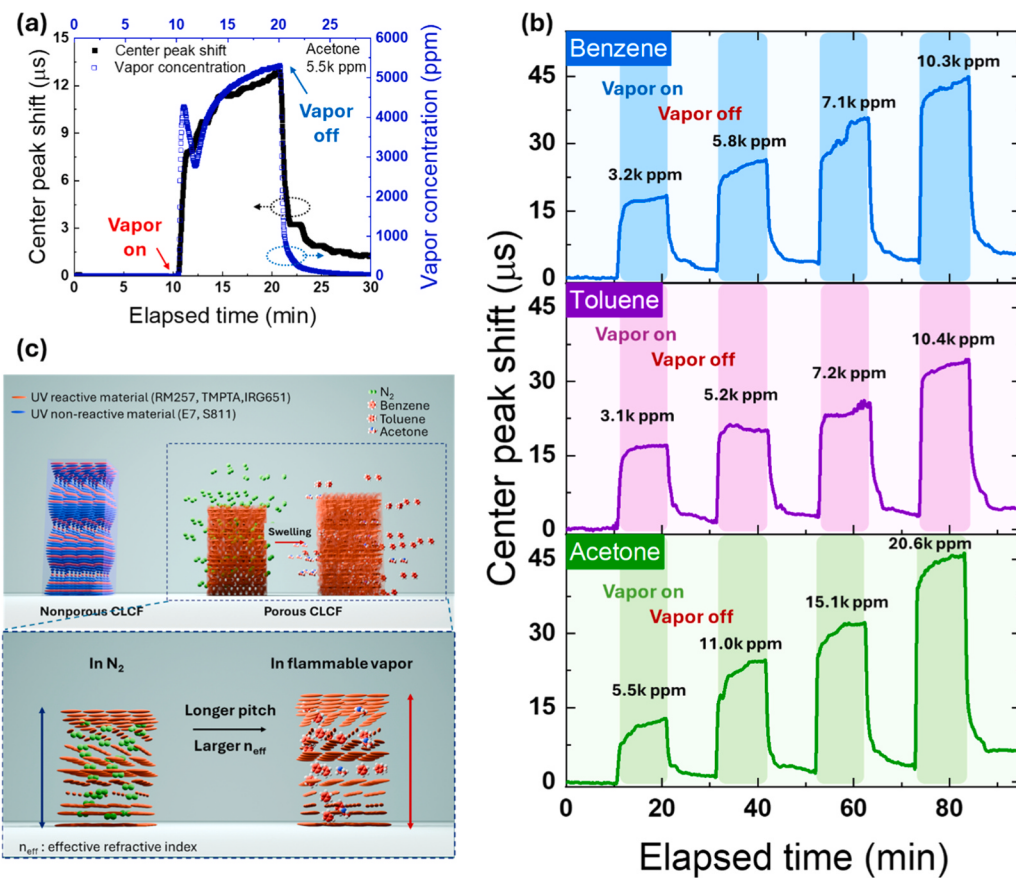


**Fig. 6.** (a) Comparison of the change in the central peak of the reflection band with respect to acetone vapor concentration during a 10-min exposure, measured using a commercial gas sensor (MP400P, blue dotted line) and the fabricated sensor element (black solid line), (b) Temporal shifts in the central peak of the reflection band as a function of vapor concentration for benzene, toluene, and acetone, measured over 10-minute response and recovery cycles, and (c) Schematic illustration of the vapor sensing mechanism in a porous CLCF.

the porous CLCF due to interactions with the material, thereby preventing a complete return to the baseline.

### 3.2. Sensing mechanism

**Fig. 6(c)** presents a schematic illustrating the vapor sensing mechanism of the porous CLCF. The sensing mechanism is primarily driven by vapor diffusion, whereby vapor molecules penetrate the porous CLCF, causing the polymer structure to swell and altering the film's effective refractive index. This vapor-induced swelling of the porous polymer is indirectly confirmed in **Fig. S5** [Supplementary material S5]. As the porous CLCF swells, the helical pitch increases and the internal effective refractive index changes, resulting in a redshift of the reflection band. Considering the hydrophobic nature of the porous CLCF, along with the dipole moments of benzene (0 D), toluene (0.36 D), and acetone (2.91 D), as well as their respective polarity indices of 2.7, 2.4, and 5.1, benzene is expected to exhibit the strongest interaction with the film due to its lowest polarity [43]. Additionally, benzene has the highest refractive index among the three vapors (benzene: 1.4844, toluene: 1.4810, acetone: 1.3544 [44,45]), which further contributes to a greater refractive index change and swelling effect. Consequently, benzene vapor is expected to produce the highest sensitivity among the tested vapors.

**Table 2** compares various previously published CLC-based VOC vapor (or gas) sensors. While existing CLC-based devices exhibit a sensitivity to acetone that is more than 10 times higher than that achieved in this study [31,33], their maximum measurable concentration is limited to several hundred ppm, making them unsuitable for detecting LEL concentrations. On the other hand, a device capable of measuring

**Table 2**  
Comparison of vapor (or gas) sensors based on the CLC.

Analyte	Sensing range (ppm)	Sensitivity (pm/ppm)	Ref.
Acetone	4.99–54.94	830	[31]
Acetone	600–500,000	0.23	[32]
Tetrahydrofuran	~ 324.50	100	[33]
Acetone	~ 726.00	60	
Methanol	~ 400.50	20	
Acetone	1040–20,600	3.19	This work
Toluene	2454–10,400	4.48	
Benzene	1445–10,300	6.11	

very high concentrations demonstrates a sensitivity that is more than 10 times higher in this study, highlighting their advantages as flammable vapor sensors [32].

### 3.3. Reliability and environmental stability of the porous CLCF coated optical fiber sensor

To confirm the repeatability of the sensing device, the response and recovery cycles for a benzene vapor concentration of 3.2k ppm (approximately 25 % LEL) were repeated five times at 10-min intervals. **Fig. 7(a)** shows the shift in the central peak of the reflection band, measured in the temporal domain. The center peak consistently shifted to nearly the same position during each response and recovery cycle. **Fig. 7(b)** displays the center wavelength of the reflection band in the spectral domain for each response, with a standard deviation of approximately 0.228 nm, demonstrating excellent repeatability and

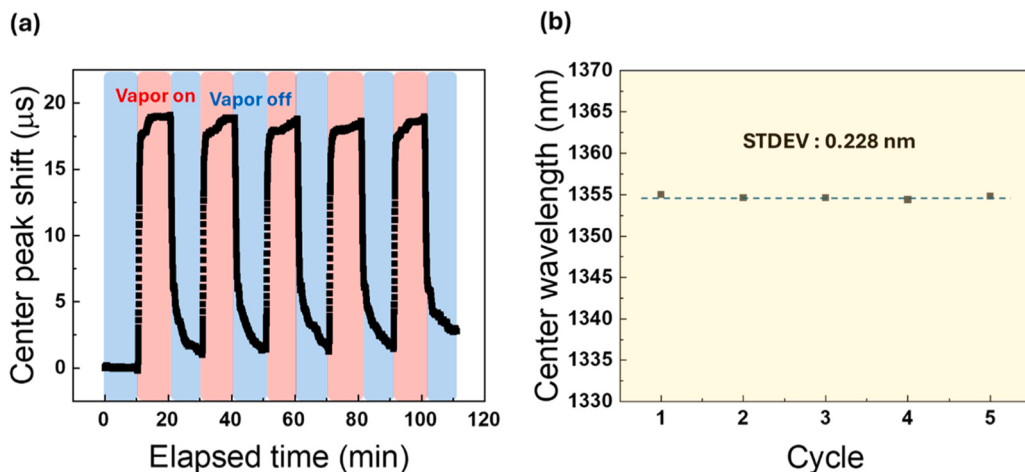


**Fig. 7.** (a) Changes in the central peak of the reflection band in the temporal domain and (b) center wavelength in the spectral domain during repeated response and recovery cycles to 3.2k ppm benzene vapor (five cycles).

short-term stability.

To evaluate the temperature and humidity dependence of the porous CLCF device, the temperature of the device was increased from 20 to 70 °C in 5 °C increments, and the relative humidity was increased from 20 % R.H. to 70 % R.H. in 5 % R.H. increments, while measuring the center wavelength of the reflection band respectively. Fig. 8 shows the center wavelength variation with temperature and humidity, respectively. The inset of Fig. 8 shows the spectra of the center wavelength according to the temperature and relative humidity change. The black squares represent the shift in the central peak of the reflected wavelength due to temperature variations, whereas the red circles indicate the shift caused by changes in humidity. As temperature changed, the center wavelength changed from 1276.6 to 1281.6 nm, and for relative humidity changed, the center wavelength changed from 1277.6 to 1281.8 nm. The center wavelength changed by about  $\pm 5$  nm over the temperature and relative humidity ranges, respectively, which represent relatively minor changes compared to the wavelength shift observed at 25 % LEL of flammable vapors. The minimal change with respect to temperature can be attributed to the fact that the porous CLCF is composed solely of polymers, with the temperature-sensitive nematic LCs removed. As a result, the changes are driven only by the thermal expansion of the polymer. Given that the porous CLCF has a regularly aligned structure and is formed by a polymer network, its thermal

expansion is expected to be minimal. The change in effective refractive index occurs when different molecules infiltrate the pores. Since the porous CLCF used in this study is hydrophobic and has a low surface energy, infiltration by nonpolar molecules is expected to be much more active compared to polar molecules. Therefore, it is anticipated that the response to relative humidity will be minimal.

#### 3.4. Comparison of the response between porous and nonporous CLCF coated optical fiber sensors

The responses of nonporous and porous CLCF devices to flammable vapors were compared by measuring the shift in the center wavelength of the reflection band for the nonporous CLCF device upon exposure to benzene vapor. Fig. 9 illustrates the change in the center wavelength of the nonporous CLCF reflection band as a function of benzene vapor concentration. When exposed to concentrations ranging from 3.4k ppm to 10.7k ppm, the center wavelength of the reflection band shifted to shorter wavelengths, from 1386.6 nm to 1376.0 nm. Additionally, the reflectivity decreased by approximately 5 % as the benzene concentration increased, likely due to the nematic LCs within the device becoming more disordered in response to the vapor.

The sensitivity of the nonporous CLCF was determined to be  $-1 \text{ pm}/\text{ppm}$  based on linear fitting, which is more than six times lower than that of the porous CLCF device. The shift of the reflection band toward shorter wavelengths and the lower sensitivity are likely due to the smaller surface area available for vapor interaction, given the absence of pores. Furthermore, the refractive index of benzene vapor is lower than that of the nonporous CLCF, causing the reflection band to shift toward

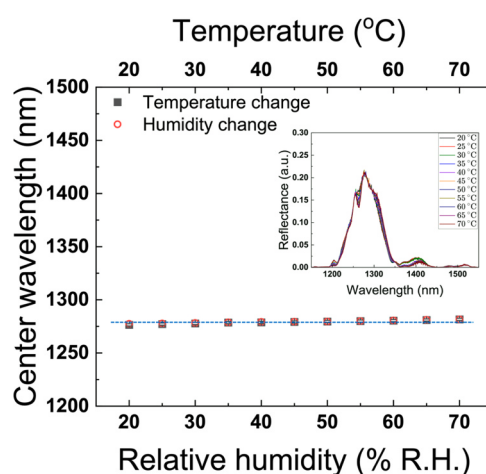


**Fig. 8.** For porous CLCF devices, the center wavelength of the reflection band shifts (a) when the temperature increases from 20 °C to 70 °C and (b) when the relative humidity increases from 20 % R.H. to 70 % R.H. (Insets: Optical spectra).

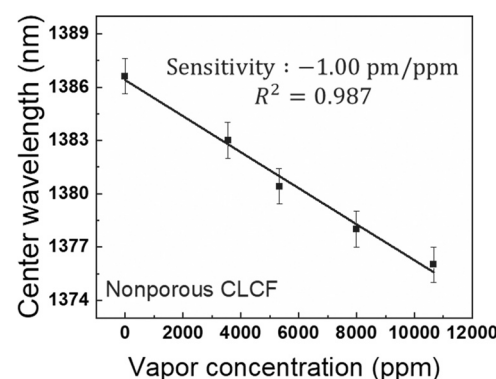


**Fig. 9.** Shift in the center wavelength of the reflection band in response to benzene vapor in the nonporous CLCF device.

shorter wavelengths.

#### 4. Conclusion

Flammable VOCs are commonly used in various industrial environments, and their evaporation can lead to vapor concentrations that approach or exceed the flammability limit. At these concentrations, even a small ignition source can cause combustion or explosions. Therefore, real-time detection of flammable VOC vapor concentration is very important to ensure the safety of industrial environments or human hazards. In this study, we successfully implemented an all-fiber optic sensor device capable of real-time detection of flammable VOC vapors by coating the cross-section of an optical fiber ferrule with porous CLCF. The reflection band changes of the porous CLCF device with varying concentrations of benzene, toluene, and acetone vapors were measured using an ultra-wideband WSL with a scanning bandwidth exceeding 440 nm as a light source. The device showed sensitivities of 6.11 pm/ppm, 4.48 pm/ppm, and 3.19 pm/ppm for benzene, toluene, and acetone, respectively, and showed the highest sensitivity for benzene vapor.

Furthermore, the ability of the WSL to establish a one-to-one correspondence between the spectral and temporal domains enabled real-time vapor concentration measurements. The sensor exhibited excellent repeatability, with a standard deviation of 0.228 nm in the reflection band at center wavelength after five consecutive exposures to 25% LEL benzene vapor. The porous CLCF device was approximately six times more sensitive than its nonporous counterpart. These findings demonstrate the potential of the proposed sensor as a reliable flammable VOC vapor detector, with the added advantages of battery-free operation, immunity to electromagnetic interference, and minimal temperature and humidity dependence.

#### CRediT authorship contribution statement

**Min Yong Jeon:** Writing – review & editing, Visualization, Validation, Supervision, Funding acquisition, Conceptualization. **Soyeon Ahn:** Writing – original draft, Validation, Methodology, Investigation, Data curation, Conceptualization. **Moon-Deock Kim:** Formal analysis. **Jong-Hyun Kim:** Formal analysis. **Minjun Kim:** Formal analysis. **Byeong Kwon Choi:** Formal analysis. **Ji Su Kim:** Formal analysis. **Min Su Kim:** Investigation, Data curation. **Nahyeon Hwang:** Visualization, Investigation, Data curation. **Na-Hyun Bak:** Formal analysis. **Jaehyun Yoo:** Formal analysis. **Sung Yoon Cho:** Formal analysis.

#### Declaration of Competing Interest

The authors declare that they have no known competing financial interests or personal relationships that could have appeared to influence the work reported in this paper.

#### Acknowledgments

This research was supported by Basic Science Research Program through the National Research Foundation of Korea (NRF) funded by the Ministry of Education (RS-2020-NR049597), by Creation of the quantum information science R&D ecosystem (based on human resources, RS-2023-00256050) through the National Research Foundation of Korea (NRF) funded by the Korean government (Ministry of Science and ICT (MSIT)), and in part by Korea Evaluation Institute of Industrial Technology (KEIT) through funded by the Korean Government (MOTIE) under Grant RS-2024-00432036; and in part by Korea Institute for Advancement of Technology (KIAT) through funded by the Korean Government (MOTIE) [Development of Regional Innovation Cluster (RIC)] under Grant P0024164.

#### Declaration of Competing Interest

The authors report no declaration of interest.

#### Appendix A. Supporting information

Supplementary data associated with this article can be found in the online version at doi:10.1016/j.snb.2025.138509.

#### Data availability

Data will be made available on request.

#### References

- [1] A. Makeenkov, I. Lapitskiy, A. Somov, A. Baranov, Flammable gases and vapors of flammable liquids: monitoring with infrared sensor node, *Sens. Actuators B Chem.* 209 (2015) 1102–1107, <https://doi.org/10.1016/j.snb.2014.11.112>.
- [2] I.A. Levitsky, Porous silicon structures as optical gas sensors, *Sensors* 15 (2015) 19968–19991, <https://doi.org/10.3390/s150819968>.
- [3] P. Saxena, P. Shukla, A review on recent developments and advances in environmental gas sensors to monitor toxic gas pollutants, *Environ. Prog. Sustain. Energy* 42 (2023) 14126, <https://doi.org/10.1002/ep.14126>.
- [4] Y. Kong, Y. Li, X. Cui, L. Su, D. Ma, T. Lai, L. Yao, X. Xiao, Y. Wang, SnO<sub>2</sub> nanostructured materials used as gas sensors for the detection of hazardous and flammable gases: a review, *Nano. Mater. Sci.* 4 (2022) 339–350, <https://doi.org/10.1016/j.nanoms.2021.05.006>.
- [5] A. Baranov, T. Osipova, Latest progress in sensors for pre-explosive detection of flammable gases: a review, *Sens. Mater.* 34 (2022) 3707–3726, <https://doi.org/10.18494/SAM405>.
- [6] I.I. Ivanov, A.M. Baranov, D.N. Spirjakin, S. Akbari, S.M. Mironov, H. Karami, G. B. Gharehpétian, Expanding catalytic sensor capabilities to combustible gas mixtures monitoring, *Measurement* 194 (2022) 111103, <https://doi.org/10.1016/j.measurement.2022.111103>.
- [7] P.G.D. Gennes, J. Prost, *The Physics of Liquid Crystals*, second ed., Oxford University Press, Oxford, 1993.
- [8] W. Zhang, A.A.F. Froyen, A.P.H.J. Schenning, G. Zhou, M.G. Debije, L.T. de Haan, Temperature-responsive photonic devices based on cholesteric liquid crystals, *Adv. Photonics Res.* 2 (2021) 2100016, <https://doi.org/10.1002/adpr.202100016>.
- [9] S. Ahn, G.H. Lee, L. Jun-Yong, Y. Kim, K. Min Su, S. Pagidi, C. Byeong Kwon, K. Ji Su, K. Jong-Hyun, J. Min Yong, Fiber-optic temperature sensor using cholesteric liquid crystals on the optical fiber ferrules, *Sensors* 22 (2022) 5752, <https://doi.org/10.3390/s22155752>.
- [10] J. Xiang, A. Varanytsia, F. Minkowski, D.A. Paterson, J.M.D. Storey, C.T. Imrie, O. D. Lavrentovich, P. Palffy-Muhoray, Electrically tunable laser based on oblique heliconical cholesteric liquid crystal, *Proc. Natl. Acad. Sci.* 113 (2016) 12925–12928, <https://doi.org/10.1073/pnas.1612212113>.
- [11] H.-G. Lee, S. Munir, S.-Y. Park, Cholesteric liquid crystal droplets for biosensors, *ACS Appl. Mater. Interfaces* 8 (2016) 26407–26417, <https://doi.org/10.1021/acsm.6b09624>.
- [12] A. Mujahid, H. Stathopoulos, P.A. Lieberzeit, F.L. Dickert, Solvent vapour detection with cholesteric liquid crystals-optical and mass-sensitive evaluation of the sensor mechanism, *Sensors* 10 (2010) 4887–4897, <https://doi.org/10.3390/s100504887>.
- [13] Y. Yang, D. Zhou, X. Liu, Y. Liu, S. Liu, P. Miao, Y. Shi, W. Sun, Optical fiber sensor based on a cholesteric liquid crystal film for mixed VOC sensing, *Opt. Express* 28 (2020) 31872–31881, <https://doi.org/10.1364/OE.405627>.
- [14] C. Esteves, E. Ramou, A.R.P. Porteira, A.J. Moura Barbosa, A.C.A. Roque, Seeing the unseen: the role of liquid crystals in gas-sensing technologies, *Adv. Opt. Mater.* 8 (2020) 1902117, <https://doi.org/10.1002/adom.201902117>.
- [15] J. Liu, W. Tai, D. Wang, J. Su, Y. Li, Cholesteric liquid crystal photonic hydrogel films immobilized with urease used for the detection of Hg<sup>2+</sup>, *Chemosensors* 10 (2022) 140, <https://doi.org/10.3390/chemosensors10040140>.
- [16] J. Hu, D. Zhou, Y. Su, S. Liu, P. Miao, Y. Shi, W. Sun, Y. Liu, Fiber micro-tip temperature sensor based on cholesteric liquid crystal, *Opt. Lett.* 45 (2020) 5209–5212, <https://doi.org/10.1364/OL.402473>.
- [17] H.O. Cirkinoglu, H. Bilgin, F. Civitci, H. Torun, O. Ferhanoglu, Fiber temperature sensor utilizing a thermomechanical MEMS detector, *J. Lightw. Technol.* 34 (2016) 1025–1030, <https://doi.org/10.1109/jlt.2015.2502992>.
- [18] W. Jin, J. Ma, F. Yang, H.L. Ho, Fiber-optic acoustic and pressure sensors with ultra-high sensitivity, in: 2013 12th Int. Conf. Opt. Commun. (ICOCN), 2013, pp. 1–3, <https://doi.org/10.1109/ICOCN.2013.6617193>.
- [19] H. Bae, M. Yu, Miniature Fabry-Perot pressure sensor created by using UV-molding process with an optical fiber based mold, *Opt. Express* 20 (2012) 14573–14583, <https://doi.org/10.1364/OE.20.014573>.
- [20] D. López-Torres, A. Lopez-Aldaba, C.E. Aguado, J.L. Auguste, R. Jamier, P. Roy, M. López-Amo, F.J. Arregui, Sensitivity optimization of a microstructured optical fiber ammonia gas sensor by means of tuning the thickness of a metal oxide nano-coating, *IEEE Sens. J.* 19 (2019) 4982–4991, <https://doi.org/10.1109/JSEN.2019.2901361>.
- [21] B.K. Choi, J.S. Kim, S. Ahn, S.Y. Cho, M.S. Kim, J. Yoo, M.Y. Jeon, Simultaneous temperature and strain measurement in fiber Bragg grating via wavelength-swept

- laser and machine learning, *IEEE Sens. J.* 24 (2024) 27516–27524, <https://doi.org/10.1109/JSEN.2024.3429366>.
- [22] Y. Zhao, Y. Liu, B. Han, M. Wang, Q. Wang, Y.-n Zhang, Fiber optic volatile organic compound gas sensors: a review, *Coord. Chem. Rev.* 493 (2023) 215297, <https://doi.org/10.1016/j.ccr.2023.215297>.
- [23] P.T. Arasu, A.L. Khalaf, S.H.A. Aziz, M.H. Yaacob, A.S.M. Noor, Optical fiber based ammonia gas sensor with carbon nanotubes sensing enhancement, in: *Proc. 2017 IEEE Reg. 10 Symp. TENSYMP 2017*, 2017, pp. 1–4, <https://doi.org/10.1109/TENCONSpring.2017.8069983>.
- [24] B.C. Yao, Y. Wu, A.Q. Zhang, Y.J. Rao, Z.G. Wang, Y. Cheng, Y. Gong, W.L. Zhang, Y.F. Chen, K.S. Chiang, Graphene enhanced evanescent field in microfiber multimode interferometer for highly sensitive gas sensing, *Opt. Express* 22 (2014) 28154–28162, <https://doi.org/10.1364/OE.22.028154>.
- [25] G. Yan, A.P. Zhang, G. Ma, B. Wang, B. Kim, J. Im, S. He, Y. Chung, Fiber-optic acetylene gas sensor based on microstructured optical fiber bragg gratings, *IEEE Photonics Technol. Lett.* 23 (2011) 1588–1590, <https://doi.org/10.1109/lpt.2011.2164575>.
- [26] C. Yao, L. Xiao, S. Gao, Y. Wang, P. Wang, R. Kan, W. Jin, W. Ren, Sub-ppm CO detection in a sub-meter-long hollow-core negative curvature fiber using absorption spectroscopy at 2.3 μm, *Sens. Actuators B Chem.* 303 (2020), <https://doi.org/10.1016/j.snb.2019.127238>.
- [27] B. Xu, J. Huang, L. Ding, H. Zhang, H. Zhang, A sensitive ammonia sensor using long period fiber grating coated with graphene oxide/cellulose acetate, *IEEE Sens. J.* 21 (2021) 16691–16700, <https://doi.org/10.1109/JSEN.2021.3089382>.
- [28] I. Vitoria, C. Ruiz Zamarreno, A. Ozcariz, I.R. Matias, Fiber optic gas sensors based on lossy mode resonances and sensing materials used therefor: a comprehensive review, *Sensors* 21 (2021) 731, <https://doi.org/10.3390/s21030731>.
- [29] L. Guo, H. Bao, F. Chen, P. Zhao, S. Jiang, H.L. Ho, W. Jin, Ultra-compact optical fiber gas sensor with high sensitivity, fast response and large dynamic range, *J. Lightw. Technol.* 42 (2024) 2617–2624, <https://doi.org/10.1109/jlt.2023.3337411>.
- [30] G. Chen, J. Li, H. Zhu, Y. Wang, H. Ji, F. Meng, Optical fiber gas sensor with multi-parameter sensing and environmental anti-interference performance, *J. Ind. Inf. Integr.* 38 (2024) 100565, <https://doi.org/10.1016/j.jii.2024.100565>.
- [31] J. Hu, Y. Chen, Z. Ma, L. Zeng, D. Zhou, Z. Peng, W. Sun, Y. Liu, Temperature-compensated optical fiber sensor for volatile organic compound gas detection based on cholesteric liquid crystal, *Opt. Lett.* 46 (2021) 3324–3327, <https://doi.org/10.1364/OL.427606>.
- [32] Y. Li, Z. Yin, D. Luo, Pre-compressed polymer cholesteric liquid crystal based optical fiber VOC sensor with high stability and a wide detection range, *Opt. Express* 30 (2022) 32822–32832, <https://doi.org/10.1364/OE.470518>.
- [33] J. Tang, J. Fang, Y. Liang, B. Zhang, Y. Luo, X. Liu, Z. Li, X. Cai, J. Xian, H. Lin, W. Zhu, H. Guan, H. Lu, J. Zhang, J. Yu, Z. Chen, All-fiber-optic VOC gas sensor based on side-polished fiber wavelength selectively coupled with cholesteric liquid crystal film, *Sens. Actuators B Chem.* 273 (2018) 1816–1826, <https://doi.org/10.1016/j.snb.2018.06.105>.
- [34] Saktioto, Y. Zairmi, V. Veriyanti, W. Candra, R.F. Syahputra, Y. Soerbakti, V. Asyana, D. Irawan, Okfalsa, H. Hairi, N.A. Hussein, Syamsudhuha, S. Anita, Birefringence and polarization mode dispersion phenomena of commercial optical fiber in telecommunication networks, *J. Phys. Conf. Ser.* 1655 (2020), <https://doi.org/10.1088/1742-6596/1655/1/012160>.
- [35] G.H. Lee, S. Ahn, M.S. Kim, S.W. Lee, J.S. Kim, B.K. Choi, S. Pagidi, M.Y. Jeon, Output characterization of 220 nm broadband 1250 nm wavelength-swept laser for dynamic optical fiber sensors, *Sensors* 22 (2022) 8867, <https://doi.org/10.3390/s22228867>.
- [36] J. Wang, A. Jäkli, J.L. West, Liquid crystal/polymer fiber mats as sensitive chemical sensors, *J. Mol. Liq.* 267 (2018) 490–495, <https://doi.org/10.1016/j.molliq.2018.01.051>.
- [37] International Labour Organization (ILO), International Chemical Safety Card: Benzene (ICSC 0015), [https://chemicalsafety.ilo.org/dyn/icsc/showcard.display?\\_p\\_lang=en&p\\_card\\_id=0015&p\\_version=2](https://chemicalsafety.ilo.org/dyn/icsc/showcard.display?_p_lang=en&p_card_id=0015&p_version=2) (Accessed 25 July 2025).
- [38] International Labour Organization (ILO), International Chemical Safety Card: Toluene (ICSC 0078), [https://chemicalsafety.ilo.org/dyn/icsc/showcard.display?\\_p\\_lang=en&p\\_card\\_id=0078&p\\_version=2](https://chemicalsafety.ilo.org/dyn/icsc/showcard.display?_p_lang=en&p_card_id=0078&p_version=2) (Accessed 25 July 2025).
- [39] International Labour Organization (ILO), International Chemical Safety Card: Acetone (ICSC 0087), [https://chemicalsafety.ilo.org/dyn/icsc/showcard.display?\\_p\\_lang=en&p\\_card\\_id=0087&p\\_version=2](https://chemicalsafety.ilo.org/dyn/icsc/showcard.display?_p_lang=en&p_card_id=0087&p_version=2) (Accessed 25 July 2025).
- [40] C. Liu, H. Chen, Q. Chen, Y. Zheng, Z. Gao, X. Fan, B. Wu, P.P. Shum, An ultra-high sensitivity methane gas sensor based on vernier effect in two parallel optical fiber Sagnac loops, *Opt. Commun.* 540 (2023), <https://doi.org/10.1016/j.optcom.2023.129509>.
- [41] A. Moshayedi, E. Kazemi, M. Tabatabaei, L. Liao, Brief modeling equation for metal-oxide; TGS type gas sensors, *Filomat* 34 (2020) 4997–5008, <https://doi.org/10.2298/fil2015997m>.
- [42] E. Kazemi, D. Sadrian Zadeh, B. Moshiri, Metal-oxide-semiconductor sensors modeling using ordered weighted averaging (OWA) operators in electronic nose, *Measurement* 184 (2021) 109932, <https://doi.org/10.1016/j.measurement.2021.109932>.
- [43] C.-P. Li, M. Du, Role of solvents in coordination supramolecular systems, *Chem. Commun.* 47 (2011) 5958–5972, <https://doi.org/10.1039/C1CC10935A>.
- [44] K. Moutzouris, M. Papamichael, S.C. Betsis, I. Stavrakas, G. Hloupis, D. Triantis, Refractive, dispersive and thermo-optic properties of twelve organic solvents in the visible and near-infrared, *Appl. Phys. B* 116 (2013) 617–622, <https://doi.org/10.1007/s00340-013-5744-3>.
- [45] J. Rheims, J. Köser, T. Wriedt, Refractive-index measurements in the near-IR using an Abbe refractometer, *Meas. Sci. Technol.* 8 (1997) 601, <https://doi.org/10.1088/0957-0233/8/6/003>.

**Soyeon Ahn** received an M. S. degree in physics from Chungnam National University, Daejeon, Republic of Korea, in 2021, where she is currently pursuing a Ph.D. degree with the Fiber Optics Laboratory, Department of Physics. Her research interests include optical fiber sensors, gas sensors, and liquid crystals.



**Nahyeon Hwang** received a B.S. degree in physics from Chungnam National University, Daejeon, Republic of Korea, where she is currently pursuing an M.S. degree with the Fiber Optics Laboratory, Department of Physics. Her research interests include cholesteric liquid crystal elastomers and strain sensors.



**Min Su Kim** received a B.S. degree in physics from Chungnam National University, Daejeon, Republic of Korea, in 2022, where he is currently pursuing an M.S. degree with the Fiber Optics Laboratory, Department of Physics. His research interests include dynamic fiber sensors, wavelength-swept lasers, and their applications.



**Ji Su Kim** received an M.S. degree in physics from Chungnam National University, Daejeon, Republic of Korea, in 2017, where she is currently pursuing a Ph.D. degree with the Fiber Optics Laboratory, Department of Physics. Her research interests include mode-locked fiber lasers, THz spectroscopy, and metasurface devices.



**Byeong Kwon Choi** received his M.S. and Ph.D in physics from Chungnam National University, Daejeon, Republic of Korea, in 2015 and 2024, respectively, and later joined Siemens EDA. His research interests include dynamic fiber sensors, wavelength-swept lasers, and their applications.



**Sung Yoon Cho** received an M.S. degree in physics from Chungnam National University, Daejeon, Republic of Korea, in 2018, where he is currently pursuing a Ph.D. degree with the Fiber Optics Laboratory, Department of Physics. His research interests include dynamic fiber sensors, wavelength-swept lasers, and their applications.



**Minjun Kim** received a Ph.D. degree in physics from Chungnam National University, Daejeon, Republic of Korea, in 2024. He is Postdoctoral Researcher with the Institute of Quantum Systems (IQS), Chungnam National University, Daejeon, Republic of Korea. His interests include plasmonics, nanophotonics, light-matter interaction.



**Jaehyun Yoo** received a B.S. degree in physics from Chungnam National University, Daejeon, Republic of Korea, in 2022, where he is currently pursuing a Ph.D. degree with the Fiber Optics Laboratory, Department of Physics. His research interests include fiber lasers, metasurface design, and their applications.

**Jong-Hyun Kim** received a B.S. degree from Seoul National University, Korea, and M.S. and Ph.D. degrees from KAIST, Korea, respectively, all in physics. Currently he is a professor of department of Physics at Chungnam National University, Korea. His current research interests are liquid crystal alignment, colloid, and application.

**Moon-Deock Kim** received his Ph.D. in department of semiconductor physics at Dongguk University, Republic of Korea in 1994. Currently he is professor of physics department at Chungnam Nat. Univ., Republic of Korea. His current research interests are Gas sensors, Photodetectors and III-V nitride semiconductor growth and device processing including LED'S, Solar cell and High Electron mobility transistors.



**Na-Hyun Bak** received an M.S. degree in physics from Chungnam National University, Daejeon, Republic of Korea, where she is currently pursuing a Ph.D. degree in the Department of Physics. Her research interests include MEMS sensors, optical sensors, and III-nitride semiconductor devices, with a focus on AlN-based SAW gas sensors and InN-based NIR photodetectors.



**Min Yong Jeon** (M'94) received a B.S. degree from Han Yang University, Seoul, Republic of Korea, in 1988, and M.S. and Ph.D. degrees from Korea Advanced Institute of Science and Technology (KAIST), Daejeon, Republic of Korea, in 1990 and 1994, respectively, all in physics. He has been a Professor at the Department of Physics, Chungnam National University, Daejeon, since May 2003. Prior to joining Chungnam National University, he worked in the field of optical routers as a Research Scientist at the University of California, Davis, CA, USA. From 1994 to 2001, he worked in the field of optical network subsystems at the Electronics and Telecommunications Research Institute (ETRI), Daejeon. His current research interests include optical coherence tomography, wavelength-swept lasers, optical fiber sensors, and optical terahertz wave generation. Prof. Jeon is a member of IEEE, SPIE, and KPS and a Senior Member of Optica and OSK.